EVALUATION OF MOMENT LIVE-LOAD DISTRIBUTION OF A NEXT-F BEAM BRIDGE THROUGH FIELD LOAD TESTING AND FE MODELING

Rami Bahjat, University of Massachusetts Amherst
Deidre Ericson, Parsons Brinckerhoff
Sergio F. Breña, PhD, University of Massachusetts Amherst
Scott A. Civjan, PhD, University of Massachusetts Amherst

ABSTRACT

NEXT beam bridges have become a popular alternative for short-to-medium span bridges primarily in the northeast because of their construction safety and efficiency. The cross-section for this bridge does not specifically fall into one of the categories identified in the AASHTO LRFD Specifications for use of simplified moment live-load distribution equations. A need to define the applicability of these equations to this type of bridge prompted research into this issue. The research reported in this paper focuses on results from field testing and finite element modeling of a NEXT F beam bridge built in Massachusetts in 2012. The study was conducted to determine appropriate moment live-load distribution factors for design of this type of bridge. The research results indicate that AASHTO live-load distribution equations may be used safely for design by considering the average spacing between stems of NEXT beams as the spacing parameter in the AASHTO LRFD equations.

Keywords: Accelerated Bridge Construction, NEXT Beams, Moment Live-load Distribution, Bridge Load Testing

INTRODUCTION

Development of the northeast extreme tee (NEXT) beam for accelerated bridge construction was undertaken by the PCI Bridge Technical Committee in recent years (Culmo and Seraderian[2]). This new precast/prestressed concrete cross section is suitable for use in medium-span bridges (45 to 90 ft. long). The NEXT beam cross-section consists of a double-tee beam with integral flange of two different thicknesses (4 in. or 8 in.). By having a deck cast integrally with the beam construction activities are facilitated and formwork needed for deck placement is eliminated. Beam depths range between 24 and 36 in., web spacing is 5 ft., and the section width can be adjusted between 8 and 12 ft. The top flange thickness is 4 in. for bridges using a cast-in-place deck (NEXT-F), or 8 in. in beams that have an integral structural deck (NEXT-D). The top surface of NEXT-F beams is roughened and contains reinforcement that extends from the beam webs (typically stirrup tops) to promote composite action. The wearing surface is applied to the top of the deck in both cases.

During design and development of the NEXT beam, questions arose about the appropriate use of live-load lane distribution factors included in the *AASHTO-LRFD Specifications*[1]. The cross section did not specifically fall into any of the categories currently included in the *AASHTO-LRFD Specifications* so the PCI-NE Bridge Technical Committee developed recommendations for designers to provide a way to calculate a conservative estimate of a live-load distribution factor for these beams. Because the Accelerated Bridge Program within the Massachusetts Department of Transportation (MassDOT) is currently planning to use NEXT beams in several bridges, a memorandum was issued to temporarily guide designers on the use of live-load distribution factors that will produce conservative designs. It has been recognized, however, that live-load distribution factors appropriate for this type of beams must be developed for an increase in use and widespread acceptance. Therefore, an instrumentation program was planned for a bridge that was constructed using NEXT-F beams so that live-load distribution factors could be determined through field testing.

This paper presents the results of a load test conducted on the NEXT-F beam bridge selected to investigate the load distribution characteristics of this type of bridge. The bridge is located in Brimfield, MA, in the central region of the state. In addition to conducting a load test, the bridge response was calculated using a detailed three dimensional finite element model. Calibration of this model is also presented in this paper.

BRIDGE DESCRIPTION

The Brimfield Bridge is located in Wales Rd (Route 19) in the town of Brimfield, MA. The bridge was constructed to replace an aging bridge located over Mill Brook that had flooding susceptibility. The bridge consists of a single span bridge on integral abutments supported on six steel HP piles per abutment. The superstructure consists of six NEXT 32-F beams with an 8-in. cast-in-place structural deck. The bridge span is 66.7 ft. to centerline of bearings and has a 30° skew (Figure 1).

The bridge was constructed in two phases to maintain an open road throughout construction. The east side of the bridge was constructed first while maintaining traffic on the west lane of the existing bridge. After completion of the east half of the bridge in October 2011, work switched to the west side and traffic was routed to the completed half of the bridge. Phase I (Beams 4 through 6) was completed in October 2011, and Phase II (Beams 1 through 3) was completed in May 2012 (Figure 1). The load test was conducted at the end of May 2012 and the long-term performance program of the bridge was initiated.

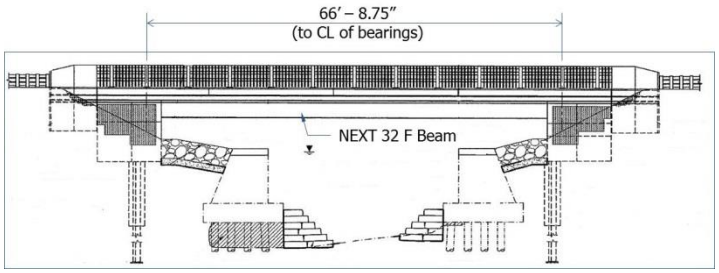

(a) Brimfield Bridge elevation

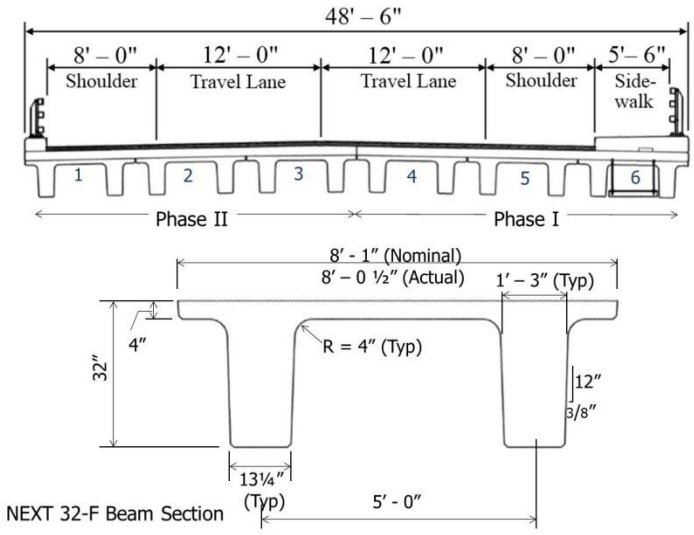

(b) Bridge cross section and dimensions of NEXT 32-F beams

Figure 1. Characteristics of Brimfield Bridge

INSTRUMENTATION

The instrumentation used in the bridge consists mostly of internal strain gauges positioned at several depths within the stems and flange of the NEXT beams, and in the cast-in-place bridge deck. Because the Brimfield Bridge is an integral abutment bridge, external instrumentation was also used to measure abutment displacements (joint meters) and rotations (tilt meters) induced during seasonal bridge contraction and expansion. Both abutments were instrumented to record differences in the displacements generated as a result of the bridge skew and possible differences in soil conditions at each end. This paper focuses

on the live-load distribution characteristics of the bridge, so only details of the instrumentation related to internal strain gauges are described in detail in this paper.

Strain gauges were positioned at three different cross-sections from the south end of the beams: a section at the third-point, a section at midspan, and a section at the two-thirds point. All beams were instrumented at midspan, whereas only beams 1 and 2 were instrumented at all three sections due to budget constraints. The strain gauges in the cast-in-place deck were placed so that they would lie directly above the beam instrumented sections at midspan or third-point sections.

Strain gauges were oriented parallel to the beam axis (longitudinal gauges) or parallel to the bridge skew angle (transverse gauges). At each instrumented section, longitudinal strain gauges were placed at three different depths within the beam and one depth in the deck to allow construction of axial strain profiles to estimate beam moments. Transverse gauges were also used at locations within the beam flange and two depths in the deck to determine transverse bending between adjacent beams. Details of the instrumentation are presented in Figure 2.

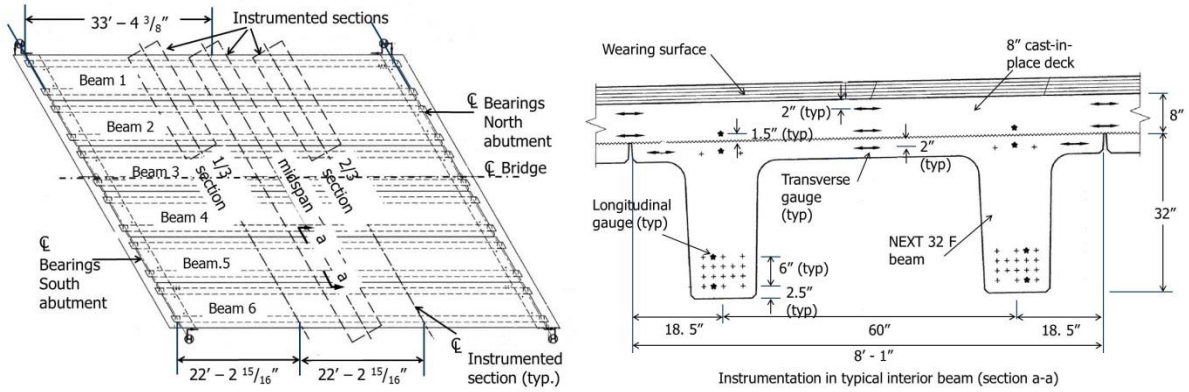

Figure 2. Instrumentation details and beam cross-section

LOAD TESTING DETAILS

The main objective of the load test was to determine the moment live-load distribution of NEXT beams. The load test was also used to calibrate a finite element model of the bridge that was used to analytically determine live-load distribution properties. The FE model and its calibration are described in a subsequent section in this paper.

LOADING CONFIGURATIONS

Static load tests were conducted by placing three loaded dump trucks at selected locations on the bridge, and maintaining them in position while data were collected. Fourteen load tests involving ten different truck configurations were chosen to generate maximum moments in selected beams or the entire bridge cross-section. In some cases, the same truck configuration was used in two different load tests by rotating the loading trucks to face either

north or south. The three dump trucks used as loading trucks were weighed and measured prior to the load test. Load tests 1 through 10 were run to maximize moments in individual girders or pairs of girders by placing trucks in a single lane; load tests 11 through 14 were designed to produce high moment on the entire bridge cross-section at midspan by placing the three trucks in a side-by-side pattern (multiple lanes). A summary of the truck configurations is listed in Table 1, and selected configurations are illustrated in Figure 3.

Table 1. Truck configurations

Test number (configuration)	Direction	Position of loading trucks	Reference tandem location*
1 (1)	South	Beam 1 – next to west curb	Midspan
2 (2)	South	Beam 2	Midspan
3 (3)	South	Beam 3	Midspan
4 (5)	South	Beam 1 and Beam 2	Midspan
5 (1)	North	Beam 1 - against west curb	Midspan
6 (2)	North	Beam 2	Midspan
7 (3)	North	Beam 3	Midspan
8 (5)	North	Beam 1 and Beam 2	Midspan
9 (6)	North	Beam 2 and Beam 3	Midspan
10 (4)	North	Beam 5	Midspan
11 (7)	North	Side by side - next to west curb	Midspan
12 (9)	North	Side by side - next to west curb	2/3 - North
13 (8)	North	Side by side - next to east curb	Midspan
14 (10)	North	Side by side - next to east curb	2/3 - North

*The tandem axle of red truck was used as reference for all configurations

LOAD TESTING DATA

For each test, data were collected from all instruments used in the bridge. Only strain data are discussed in this paper since these values were used to investigate the load distribution characteristics. Other data collected (abutment displacements and rotations) were used in support of the FE model calibration process that is described in the section on finite element modeling in this paper.

MEASURED STRAINS

Strains measured during the load test correspond only to live-load strains generated by the loading trucks. A zero reference reading was taken at the beginning of the load test before trucks were positioned on the bridge. The ambient temperature did not change significantly between beginning and ending of the load testing program, so the strain change registered in each instrument corresponds only to load-induced strain. The peak strains measured during the load tests were approximately equal to 70 με in tension and 23 με in compression. Load configurations with trucks placed side-by-side generated in general the highest strains

recorded, and also engaged a larger number of beams than configurations with trucks located over a single beam.

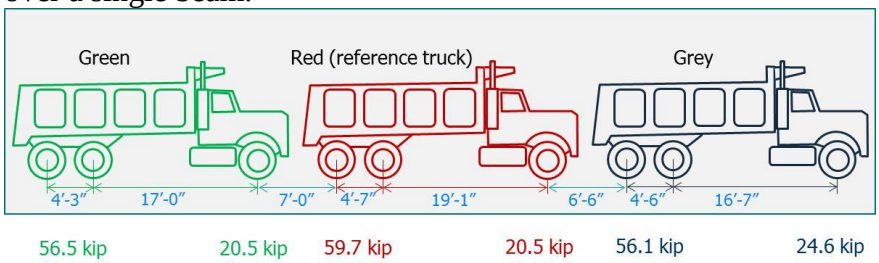

(a)

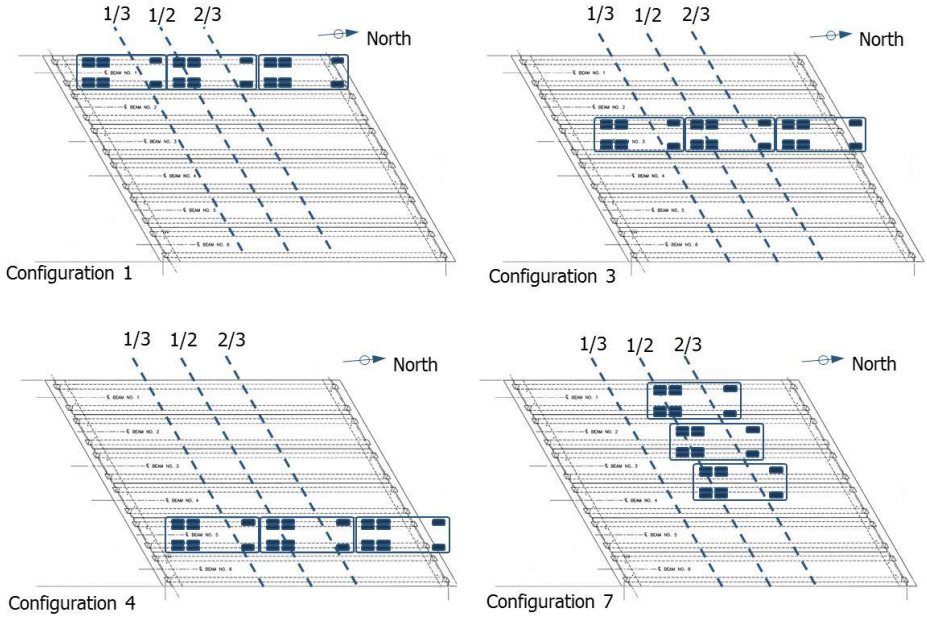

(b)

Figure 3. Load testing trucks and positions. (a) Truck dimensions and axle weights; (b) Selected north-facing truck configurations used in load test

Live-load strains measured at different depths in the beams were plotted across the bridge cross-section for each load test as an indicator of the transverse live-load distribution characteristics of the bridge. The section at midspan was fully instrumented across the bridge, so only midspan strains are presented. Figure 4 shows plots of strains measured in each web of the six bridge beams at different depths for selected load tests. Each line color maps to different depths in the cross section where strain gauges were located. Negative strains correspond to compression and positive strains are tensile.

The plots show that strains measured in the deck are compressive and strains measured in the beams are tensile. This observation is not applicable to beams farthest from the loading truck position because of the small magnitude of all strains in those cross sections. The strain distributions also indicate that the transition between compressive and tensile strains occurs near the bottom of the cast-in-place deck indicating that composite behavior was being developed between the beams and deck.

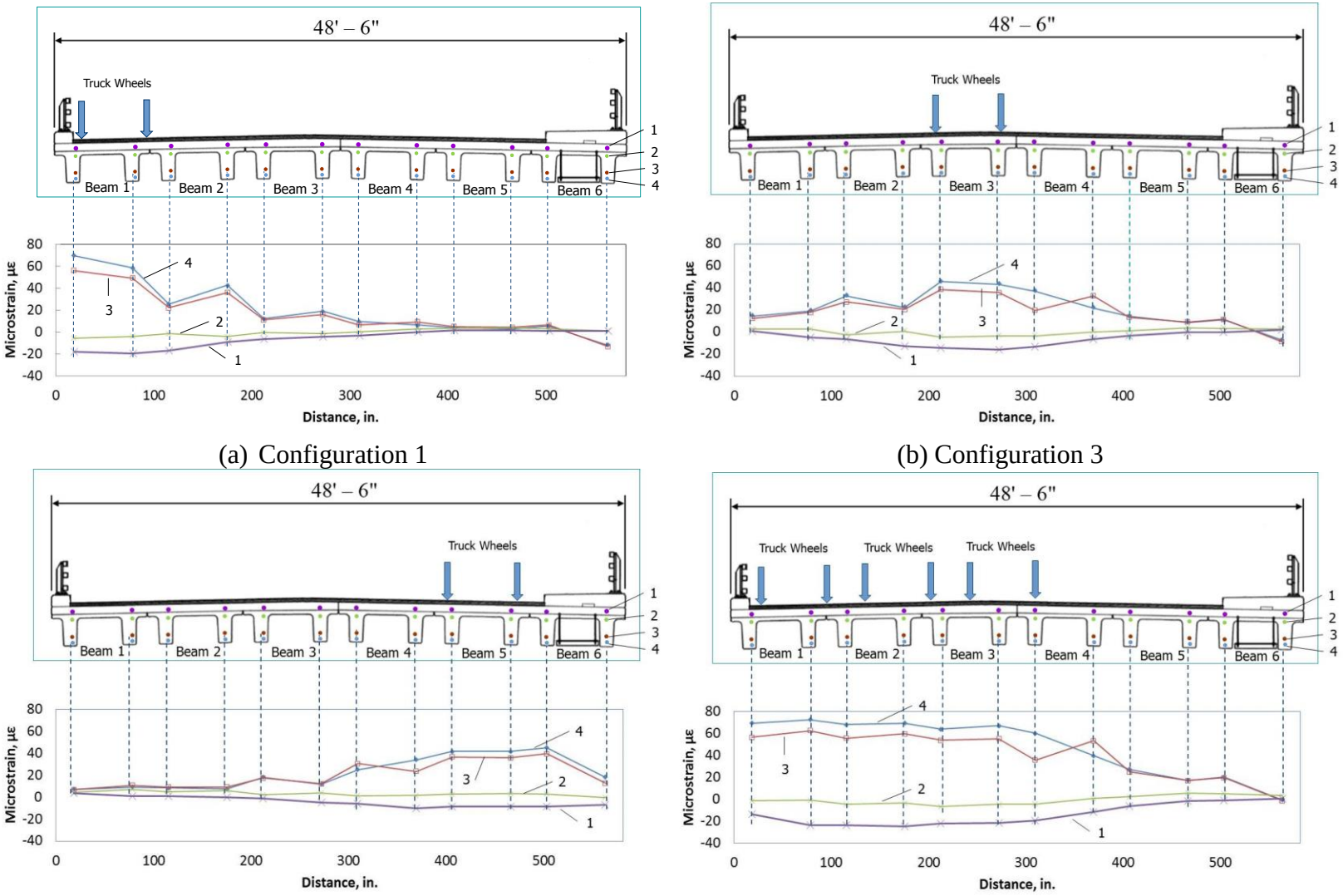

Figure 4. Axial strain distribution across bridge for selected north-facing configurations

As would be expected, strains decrease with distance from the location of applied loads, indicative of lower bending moments being developed in beams transversely far from the location of loading. However, strains did not decrease uniformly as one would intuitively anticipate, but strain drops were observed in various cases in the first web of beams adjacent to the loaded beam (for example, Beam 2 in Figure 4a and 4b; and Beam 4 in Figure 4c and 4d). The drop or increase in strain from the general trend could have been caused by torsional warping of the cross-sections resulting from eccentricity of the applied loads relative to beam centroid. Beams directly under the loading trucks did not exhibit sharp differences in strain but small differences in strain values were still observed.

Plots of strains over beam depth were constructed to identify the neutral axis location and verify linearity of strains with depth. A linear strain distribution with depth would indicate that beam behavior was governed by bending, whereas a non-linear distribution could be indicative of warping torsion effects that add or subtract from bending strains. Figure 5 shows strain-depth plots of the three beams directly under the applied truck loads in Configuration 7. The plots were generally linear for beams directly under applied loads, but turned nonlinear in beams located farther away from the loads. The beams farthest from the truck wheel loads (not shown) exhibited the most erratic distributions of strains with depth, but in these beams strain values were also the smallest. Similar observations can be made for other beams in the bridge.

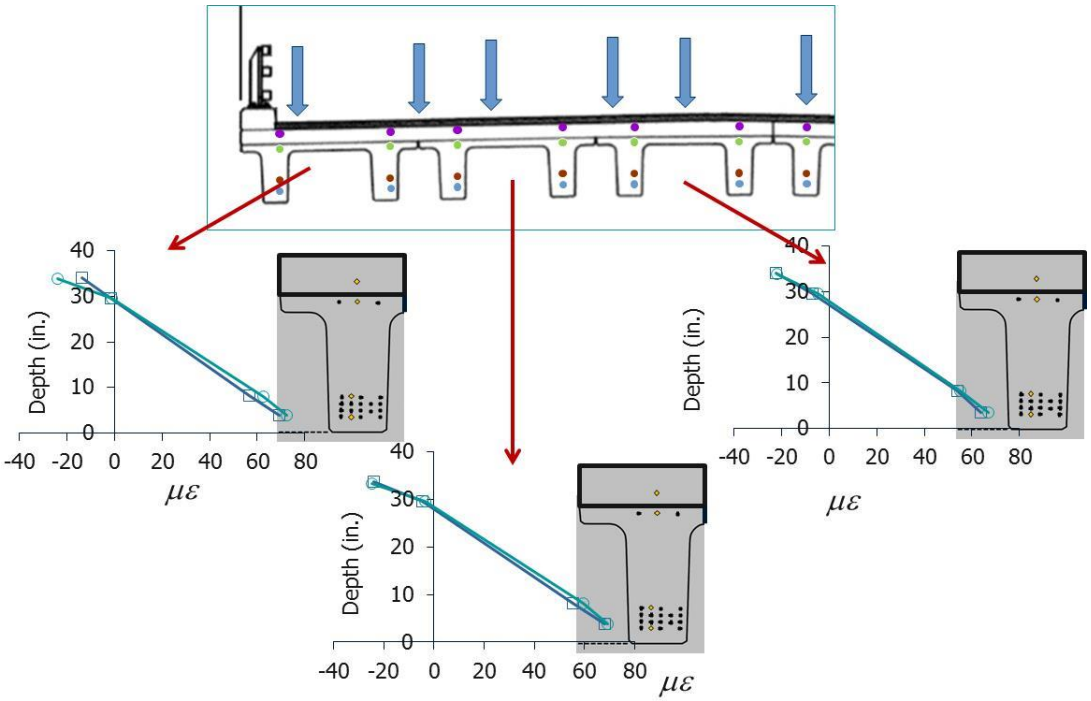

Figure 5. Strain-depth profiles for beams 1 through 3 in Configuration 7

CALCULATED MOMENTS

Measured strains were used to estimate moments generated in each beam of the bridge cross section assuming linear-elastic behavior of the bridge during the load tests. This assumption was considered reasonable given the small magnitudes of measured strains during the load tests. Moments were estimated using strains measured at the bottom strain gauge since these values were considered to be the most reliable because of their highest magnitude. To estimate moment in each NEXT beam, the bottom strains measured in each web were averaged to eliminate effects of axial strains induced by torsional warping of the cross-section. Beam moments were computed using these average strains in the bending formula:

$$M = \frac{EI \cdot \varepsilon_{avg}}{y_{bott}} \quad (1)$$

where E = modulus of elasticity of beam concrete (assumed equal to 6310 ksi); ε_{avg} = average bottom strain in the beam; I = gross moment of inertia of the composite cross-section transformed to beam concrete; and y_{bott} = distance from the neutral axis and the bottom strain gauge. The neutral axis depth was first estimated using the composite section properties of the bridge. The calculated neutral axis depth (24.3 in.) was compared with the depth determined from measured strain profiles and was found to be closer to the bottom of the beams than measured. This discrepancy was primarily a result of differences in assumed and actual beam and deck concrete strengths (and elastic moduli), and to the possible presence of axial load from restraint provided by the integral abutments. Axial force induced by truck loads was quantified using a finite element model of the bridge, and its magnitude was less than 0.1 A_g f'_c for the beams. Therefore, a neutral axis depth computed by averaging the observed location in all beams for Configurations 7 and 8 was used in all subsequent calculations (30 in. from the bottom of the beams). The observed neutral axis depth in other configurations was, in some cases, slightly lower than this value.

Plots of moments calculated in each beam for different load tests are shown in Figure 6. The plots show that beam moments decrease with distance from loading location as would be anticipated. Figure 6a shows the beam moments at midspan for four loading configurations corresponding to trucks lined up on a single lane facing the north direction of the bridge and the tandem axle of the red truck (reference) positioned at the midspan section. The difference in moment generated in the exterior beams for Configurations 1 and 4 is related to the proximity of the trucks to the edge of the bridge. The sidewalk on the east side of the bridge over beam 6 prevented trucks from being placed over the exterior beam as was done on beam 1 in Configuration 1, resulting in lower moments in beam 6 in Configuration 4.

Figure 6b compares midspan moments induced by placement of the three trucks in a side-by-side configuration with the tandem axles at two different bridge sections (midspan in Configuration 7 and two-thirds section in Configuration 9). The reduction observed in moment from west to east corresponds to the placement of trucks toward the west side. Interestingly the trends in midspan are very similar regardless of the location of the tandem

axle but, as expected, the moments are smaller when the axles are placed at the two-thirds section.

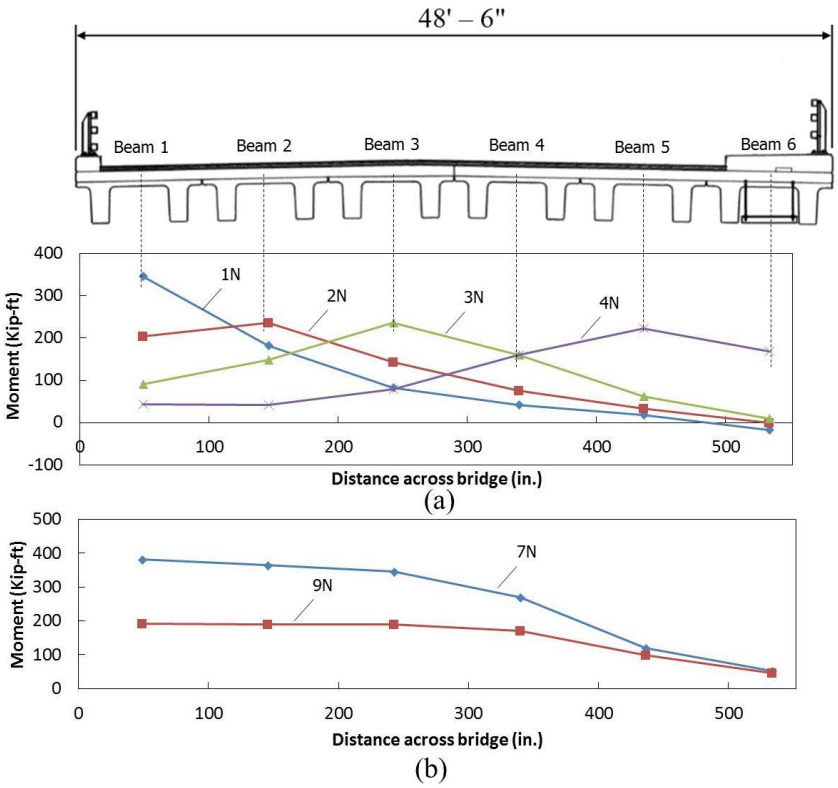

Figure 6. NEXT beam moment distribution across bridge at midspan: (a) single lane truck configurations; (b) side-by-side truck configurations

The total moment across the bridge was estimated by adding the individual moment in each beam for the different truck configuration and comparing these values with simple line models of the entire bridge, assuming fixed-fixed support conditions and simply supported end conditions. In these models, actual axle weights for each truck and their position along the bridge were used to determine the total bridge moment. As expected, the models corresponding to a fixed-fixed support assumption led to better estimates of the total moment measured in the bridge because of the integral connection of beams into abutments.

LIVE-LOAD DISTRIBUTION PROPERTIES

With the confidence gained from comparing the load-test moments to the total moment on the bridge using simple models, moment live-load distribution factors were determined for each load test. Moment live-load distribution factors were estimated by dividing the load-test moment in each beam by the total moment measured during the test. The individual beam live-load distribution factors differed from load test to load test because of the truck positioning and bridge skew. From all the load tests conducted, however, the maximum

factor obtained was compared to the design live-load distribution factor for moment obtained using equations for a single and multiple loaded lanes according to *AASHTO LRFD Specifications* (2012), given below:

$$LLDF_{1L} = \left\{0.06 + \left(\frac{S}{14}\right)^{0.4}\left(\frac{S}{L}\right)^{0.3}\left(\frac{K_g}{12Lt_s^{\,3}}\right)^{0.1}\right\}\left(1 - C_1\tan(\alpha)^{1.5}\right) \quad (2)$$

$$LLDF_{2L} = \left\{0.075 + \left(\frac{S}{9.5}\right)^{0.6}\left(\frac{S}{L}\right)^{0.2}\left(\frac{K_g}{12Lt_s^{\,3}}\right)^{0.1}\right\}\left(1 - C_1\tan(\alpha)^{1.5}\right) \quad (3)$$

Definitions for variables used in these equations may be found in the *AASHTO LRFD Specifications*[1].

To compute AASHTO live-load distribution factors, a bridge Type k was assumed with a spacing of beams equal to the average spacing between stems, S* (see Figure 7). The resulting values were multiplied times two to end up with a factor to be used for an entire beam and not individual webs.

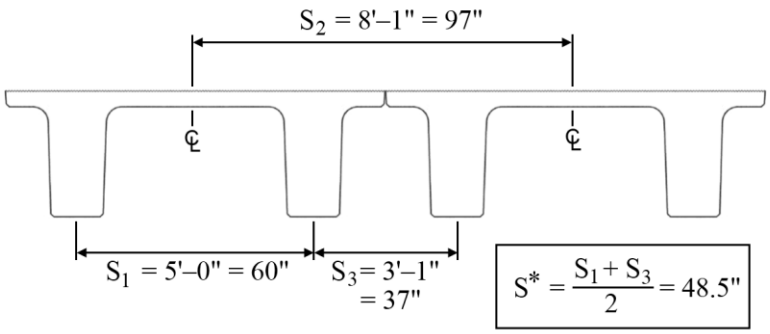

Figure 7. Spacing of beams used for AASHTO live-load distribution factor equations

Using Equations 2 and 3, moment live-load distribution factors for the Brimfield Bridge were computed to be equal to 0.61 and 0.78 for one lane and two-or-more lanes loaded, respectively.

Two conditions were considered to determine the governing moment live-load distribution factors from the load tests: (1) load-test cases consisting of trucks placed in a single lane (Configurations 1 through 7), and (2) load–test cases consisting of trucks in multiple lanes (Configurations 7 through 10). Table 2 lists moment live-load distribution factors computed for each beam under all loading configurations. The loading configurations that gave the highest (governing) live-load distribution factors are those involving trucks placed side-by-side. These configurations have a maximum live load distribution factor of 0.75 as listed in the table. These values are close, but slightly lower than the factor computed using Equation 3 (0.78) with the spacing definition in Figure 7. Further, the maximum single lane live-load distribution factor of 0.53 was also lower than the factor computed using Equation 2 (0.61).

These results indicate that the moment live-load distribution factor computed by AASHTO equations is conservative if the average stem spacing (S*) is used for NEXT F beam cross sections.

Table 2. Moment live-load distribution factors for individual beams and governing factor

Load test[a]	**Moment (Kip-ft)**							**M_{max}/M_{total}**[b]
	Beam 1	Beam 2	Beam 3	Beam 4	Beam 5	Beam 6	Total	
1N	346.05	182.04	82.21	42.30	18.67	-17.03	654.24	0.53
1S	170.08	90.02	83.74	35.87	15.83	-3.86	391.67	0.43
2N	203.36	236.45	144.07	75.29	33.54	-0.33	692.38	0.34
2S	195.56	228.99	130.37	57.11	25.53	-7.35	630.21	0.36
3N	90.58	148.10	236.40	160.12	62.03	10.43	707.66	0.33
3S	91.64	149.67	224.12	143.79	55.97	5.52	670.71	0.33
4N	44.03	41.93	79.74	159.47	223.48	168.85	717.48	0.31
5N	293.10	210.83	106.12	58.80	23.23	-8.02	684.06	0.43
5S	277.11	213.84	104.30	49.71	22.01	-13.70	653.27	0.42
6N	144.39	211.93	193.99	105.11	40.58	3.46	699.47	0.30
7N	381.76	365.98	345.54	270.30	119.26	51.28	1534.11	0.75
8N	107.53	190.66	340.26	389.69	313.84	221.26	1563.24	0.75
9N	191.40	189.32	190.49	170.82	99.17	46.54	887.73	0.65
10N	80.55	99.01	162.83	207.17	175.97	165.36	890.90	0.70
FE-7N[c]	399.04	357.61	334.36	332.50	117.50	80.63	1621.64	0.74
FE-8N[c]	94.40	254.74	332.50	396.30	404.41	163.76	1646.10	0.74

[a]Number indicates configuration number and letter indicates facing direction of trucks.
[b]The total moment in Configurations 7 through 10 was divided by three to calculate the live-load distribution factor for a single loading lane.
[c]Live-load distribution factors from FE models were only computed for variable soil conditions (see FE section in paper).

FINITE ELEMENT MODEL OF BRIMFIELD BRIDGE

A finite element (FE) model of the Brimfield Bridge was constructed to capture the response of this particular bridge, and to allow a parametric analysis of similar bridges with varying geometries. Only the procedure used to calibrate the FE model for the bridge and the method to calculate live-load distribution factors using the calibrated model are presented in this paper.

DESCRIPTION OF THE MODEL

The FE analysis program used to model the Brimfield Bridge was SAP 2000 V14.2. Details of the bridge model are divided into superstructure and substructure. The following sections discuss the modeling aspects for each of these components.

Superstructure Modeling

The NEXT 32 F beams were modeled as 3D-frame elements with 6 degrees of freedom per node. The 8-in. cast-in-place deck was modeled using 4-node quadrilateral thin shell elements. Shell element nodes that resulted from meshing the deck coincided in space and were connected to nodes in the NEXT beam frame elements. Each segment along the length of the NEXT beams was approximately 2 ft. long. The concrete deck element dimensions were defined to be consistent with nodes on the beam frame elements and to have a width-to-length ratio of approximately 1.0.

The beam and shell element nodes were defined spatially on the same horizontal plane. Shell nodes were offset to the top of the NEXT beam flange using the insertion point command in SAP 2000. The offset value was equal to 16.65 in. for the NEXT 32 F beams used in the model.

Substructure Modeling

The substructure of the bridge consists of integral abutments at both ends supported on steel HP-piles. The substructure response therefore influences the bridge response for short-term and long-term loading. Furthermore, beams were assumed to develop a monolithic connection with the abutments.

The abutments of the bridge are 4 ft. thick and have an approximate height of 11 ft. Each abutment is supported on six HP 10 x 57 steel piles oriented so that the weak axis is perpendicular to the road alignment. The abutment was modeled using 4-node thick shell elements with a length-to-width ratio between 1.5 and 2.0 to align with the location of beams and piles. The abutment height was divided into four rows of elements, with the first row corresponding to the depth of the NEXT beams in the superstructure. Each abutment element has six degrees of freedom per node.

Each pile was modeled using twenty 2-node 3D-frame elements throughout a pile length of 40 ft. The piles were pinned at their bases and were connected to abutment joints at the top.

Abutment backfill was modeled using nonlinear springs with different properties for the two halves of the bridge that were constructed in different phases. The soil properties used in each region of the abutments for construction phases I and II are described in the calibration section. Soil property differences were used to reflect possible changes in density that may have occurred between the first and second construction phases. The completed half of the bridge in phase I had undergone the first cycle of thermal loading by the time the load test was conducted after completion of phase II. Major differences in the live-load response were not anticipated since previous researchers have reported little influence of soil properties on response of integral abutment bridges subjected to live-load (Dicleli and Erhan[3]).

Nonlinear modeling of pile-soil interaction was done using force-displacement curves to represent soil restraint along the length of piles. The length of each pile segment was set at 1 ft. A force-displacement curve at each depth was calculated using the hyperbolic tangent

method used by Civjan et al.[4] in the analysis of a steel superstructure integral abutment bridge.

CALIBRATION OF THE MODEL

The FE model was calibrated using selected results of the load test. The calibration process included modification of soil spring properties used to model soil-foundation structure interaction. Initial estimates of soil spring properties were used and the model results were compared with beam moments obtained from the load tests. The soil spring properties were adjusted to better match load-test results. As mentioned earlier, the bridge was constructed in two phases, so soil density behind the abutments and top of piles could have changed after the first cycle of thermal loading that occurred between phases I and II.

Model calibration was based on comparing beam midspan moments obtained from strains measured during the load tests and moments computed in the beams using the FE model. Only load tests that generated the highest moment in the bridge cross-section were selected for the calibration process (Configurations 7 and 8) given the complexity of the calibration process and the higher variability of beam strains observed in load tests that involved trucks positioned in a single lane.

FINITE ELEMENT MODEL RESULTS

Figure 8 shows comparisons of load-test and FE beam moments for Configurations 7 and 8. The results shown correspond to the calibrated models using two different soil density conditions. In one of the models (model 1, diamond symbols), the backfill soil behind the abutments was modeled using dense properties and the soil surrounding the piles was considered mid-dense. A second model considered varying soil densities (model 2, square symbols) according to the construction phasing followed in the bridge. For the portion of the model corresponding to construction phase I, soil behind the abutment was modeled as mid-dense and the top 10 ft. of soil surrounding the piles was modeled using loose soil properties. Portions of the model corresponding to construction phase II used dense soil properties behind abutments and mid-dense soil around piles. Soil properties corresponding to each of these conditions are listed in Table 3.

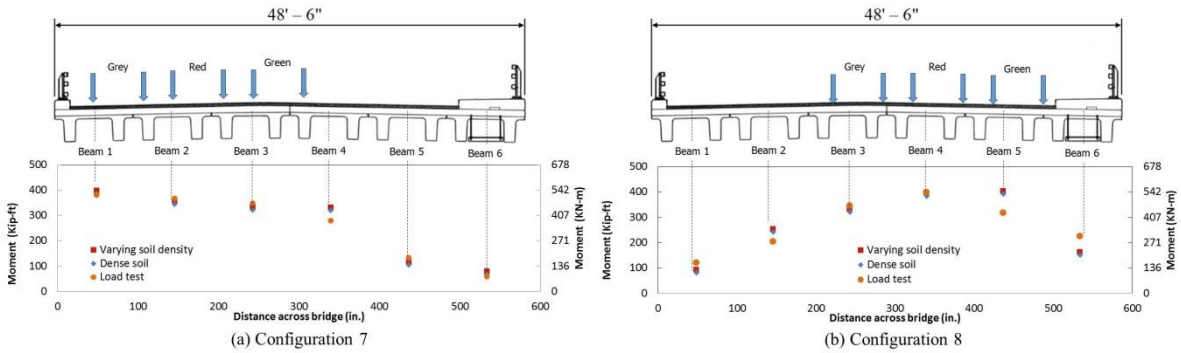

Figure 8. Beam moments determined from load tests and FE models

Table 3. Properties of soils used in different FE models

Soil type	Soil property			Use in FE models	
	Submerged unit weight, γ' (lb/ft^3)	Modulus of subgrade reaction, k_s (lb/in^3)	Angle of internal friction, ϕ' (degrees)	Model 1	Model 2
Dense (abutments)	140	NA	45	Abutment	Abutment phase II
Mid-dense (abutments)	125	NA	37	NA	Abutment phase I
Mid-dense (piles)	62.6	104	37	Piles	Top 10 ft. of piles phase II
Loose (piles)	47.6	45	30	NA	Top 10 ft. of piles phase I

Beam moments agree exceptionally well with those determined from the load tests except for moments in beams 5 and 6 in Configuration 8, attributed to the strength and stiffness contribution of the sidewalk. The discrepancies between measured and calculated moments ranged between 3 and 34 percent, with the largest difference corresponding to beam 6. Also, calculated moments matched measured values better in Configuration 7 than in Configuration 8, perhaps due to closer proximity of the loading trucks to the sidewalk in the latter configuration, which may have been influenced by the stiffness of the bridge near that side. The change in FE moments resulting from varying soil properties in abutments and piles was not significant.

The ratio between individual beam moments and the total moment in the bridge cross-section was used to calculate live-load distribution factors using the calibrated FE model. Since FE beam moments were of the same order as those obtained from the load test, the live-load distribution factors were also comparable. The difference in live-load distribution factors was not significant and values were slightly lower than those computed using AASHTO LRFD live-load distribution equations.

CONCLUSIONS

The main conclusions of the study presented in this paper are summarized below:

1. Live loads used during the load test of the Brimfield Bridge were effectively distributed across the entire bridge. The 8 in. thick deck provided the continuity necessary for live-load distribution to occur.

2. Beams directly under the application of truck loads responded primarily in bending as evidenced by a linear distribution of strain with depth of the cross-section. In contrast, the strain distribution with depth in beams adjacent to truck loads did not follow a linear trend indicating combined bending and warping.

3. Live-load distribution factors can be determined using field load testing of existing bridges by properly selecting loading configurations. Load tests are important to calibrate finite element models of the bridge to produce a high fidelity results that can be used to extend the results to other bridge geometries.

4. Given the transverse stiffness of the superstructure system, almost all beams across the bridge participated in carrying the applied truck loads resulting in much lower live-load distribution factors (0.53 compared with 0.61) than calculated using *AASHTO LRFD* equations for a single loaded lane.

5. The governing live-load distribution factor corresponded to cases involving multiple loaded lanes. Live-load distribution factors for load tests involving multiple loaded lanes (0.75) were close to those calculated using *AASHTO LRFD* equations (0.78) if a spacing parameter equal to the average spacing between stems of NEXT beams was used.

ACKNOWLEDGMENTS

The research reported in this paper was made possible through a PCI Daniel P. Jenny Student Fellowship. The Massachusetts Department of Transportation provided funding to install the instrumentation at the bridge. Contributions from PCI Northeast, the New Hampshire Department of Transportation and Central Atlantic Bridge are also gratefully acknowledged. The first author expresses gratitude for the support received from the Higher Committee for Education Development (HCED) of Iraq to pursue graduate studies.

REFERENCES

1. American Association of State Highway and Transportation Officials (AASHTO), *AASHTO LRFD Bridge Design Specifications,* 6th edition, 2012.

2. Culmo, M.P. and Seraderian, R.L. "Development of the Northeast Extreme Tee (NEXT) Beam for Accelerated Bridge Construction," *PCI Journal*, V. 55, No. 3, 2010, pp. 86–101.

3. Dicleli, M. and Erhan S. "Effect of Soil and Substructure Properties on Live-load Distribution in Integral Abutment Bridges." *ASCE J. Bridge Eng.,* V.13, No. 5, 2008, pp. 527–539.

4. Civjan S.A., Bonczar C.H., Breña S.F., DeJong J.T., and Crovo D.S. "Integral Abutment Bridge Behavior: Parametric Analysis of a Massachusetts Bridge", *ASCE J. Bridge Eng.,* V. 12, No. 1, 2007, pp. 64–71.